nature catalysis

ARTICLES

https://doi.org/10.1038/s41929-021-00654-6

Check for updates

Unusual zymogen activation patterns in the protein corona of Ca-zeolites

Xiaoqiang Shang[1,5], Hao Chen[1,5], Valentina Castagnola[2], Kai Liu[2], Luca Boselli[2], Vanya Petseva[2], Lisha Yu[1], Liping Xiao[1], Min He[3], Fangjun Wang[3], Kenneth A. Dawson[2,4] ✉ and Jie Fan[1] ✉

Zymogen (prothrombin) activation is central to the process of haemostasis (blood clotting) in the body, preventing serious blood loss and death from haemorrhagic shock. Zeolites comprise a family of crystalline microporous aluminosilicates that show increasing promise for use in massive bleeding control. However, the mechanism of zeolite-initiated haemostasis has remained unclear. Here, we investigate zeolite-initiated thrombin activation at the molecular level, and show that a prothrombinase complex can assemble on the inorganic surface of calcium-ion-exchanged zeolites (Ca-zeolites). Compared to natural platelet-based physiological processes, prothrombin-to-thrombin conversion on the surface of Ca-zeolite displays a striking thrombin activation pattern, with an exceptionally high plateau thrombin activity and at least 12-fold enhanced endogenous thrombin. The results provide a mechanistic understanding of how the zeolite surface functionally contributes to thrombin activation, paving the way towards the design of improved agents for bleeding management.

Proteases have many physiological functions, ranging from generalized protein digestion to more specific regulated processes such as zymogen activation, blood coagulation and the lysis of fibrin clots[1,2]. In the process of blood clotting, the activation of blood coagulation factors involves proteolysis of a zymogen to yield a new proteolytically active enzyme. Specifically, the conversion of the zymogen prothrombin into thrombin has a profound impact on fibrin clot formation and haemostasis. According to the cell-based model of coagulation, thrombin activation processes are divided into three sequential phases: initiation, priming and propagation[3]. The whole process occurs slowly, and optimum progression is ensured only in the presence of a prothrombinase complex, which consists of the serine protein, factor Xa, and the protein cofactor, factor Va. This complex assembles on negatively charged phospholipid membranes (platelets) in the presence of calcium ions[3–5]. Platelets provide an ideal functional surface on which (under appropriate conditions) strands of fibrin form an organized clot, providing and mediating a series of clotting factors. Thrombin activation is a key reaction in the coagulation cascade, which functions to regulate haemostasis in the body and is critical in preventing serious blood loss and death from haemorrhagic shock[6,7]. It is of great interest to explore new clinical approaches to achieving rapid haemostasis to improve the survival rates of patients with substantial bleeding.

Zeolites comprise a family of crystalline microporous aluminosilicates that are showing increasing promise as haemostatics. In the early 2000s, granular zeolite-based haemostatic agents were verified in several animal models for temporary massive bleeding control[8,9] and have been used by the US Armed Forces in the wars in Afghanistan and Iraq[10,11]. However, on application, these granular zeolite haemostats were found to cause an exothermic reaction, resulting in thermal burns and tissue necrosis, and have since been superseded by 'combat gauze' (a kaolin-based material), which circumvents this issue[12,13]. In 2019, a tightly bonded and flexible mesoporous zeolite–cotton hybrid haemostat was developed that not only overcame the exothermic reaction challenge found with zeolite-based granular haemostats, but also eliminated the potential risk of impregnated kaolin powder entering the body[14]. Zeolite–cotton hybrid haemostats were found to exhibit superior procoagulant activity over kaolin haemostats in a lethal femoral artery injury rabbit model, displaying a much shorter clotting time and lower blood loss (40% less). However, the mechanism of zeolite-initiated haemostasis remained unclear. The prevailing view is that protein coagulation factors are concentrated by water adsorption, and calcium ions are released to prime the surface[15]. This hypothesized mechanism oversimplifies the haemostasis process and fails to explain the super procoagulant activity of the protein corona-zeolite composite[16].

We have long been aware that the nature of the protein corona on inorganic materials, including zeolites, depends on parameters such as particle size, various bare material surface properties (for example, charge and topological structure), as well as the kinetic processes of adsorption[17–20]. Selective adsorption of biomolecules can transform the surface of a particle and determine subsequent physiological responses by activating specific receptors or immunoglobulins[21–24]. This determines the final in vivo identities of the nanomaterials[25,26]. However, the role of kinetic control of adsorption in corona formation is less well understood, and the concept of active kinetic programming, in which the nanoparticle surface initiates pre-programmed surface adsorption or a zymogen activation event sequence, is an intriguing and potentially important new dimension.

In this Article, we resolve the evolution of the hard protein corona (HPC)[27] in Ca-zeolite-initiated haemostasis, and trace the localization and activation of specific coagulation factors during the evolution period. We investigate zeolite-initiated coagulation at the molecular level, and follow the physiological coagulation cascade on a timescale of minutes. We thereby derive a model of the

[1]Key Lab of Applied Chemistry of Zhejiang Province, Department of Chemistry, Zhejiang University, Hangzhou, China. [2]Centre for BioNano Interactions (CBNI), School of Chemistry, University College Dublin, Dublin, Ireland. [3]Key Laboratory of Separation Sciences for Analytical Chemistry, National Chromatographic R&A Center, Dalian Institute of Chemical Physics, Chinese Academy of Sciences, Dalian, China. [4]Guangdong Provincial Education Department Key Laboratory of Nano-Immunoregulation Tumour Microenvironment, The Second Affiliated Hospital, Guangzhou Medical University, Guangzhou, Guangdong, P. R. China. [5]These authors contributed equally: Xiaoqiang Shang, Hao Chen. ✉e-mail: kenneth.a.dawson@cbni.ucd.ie; jfan@zju.edu.cn

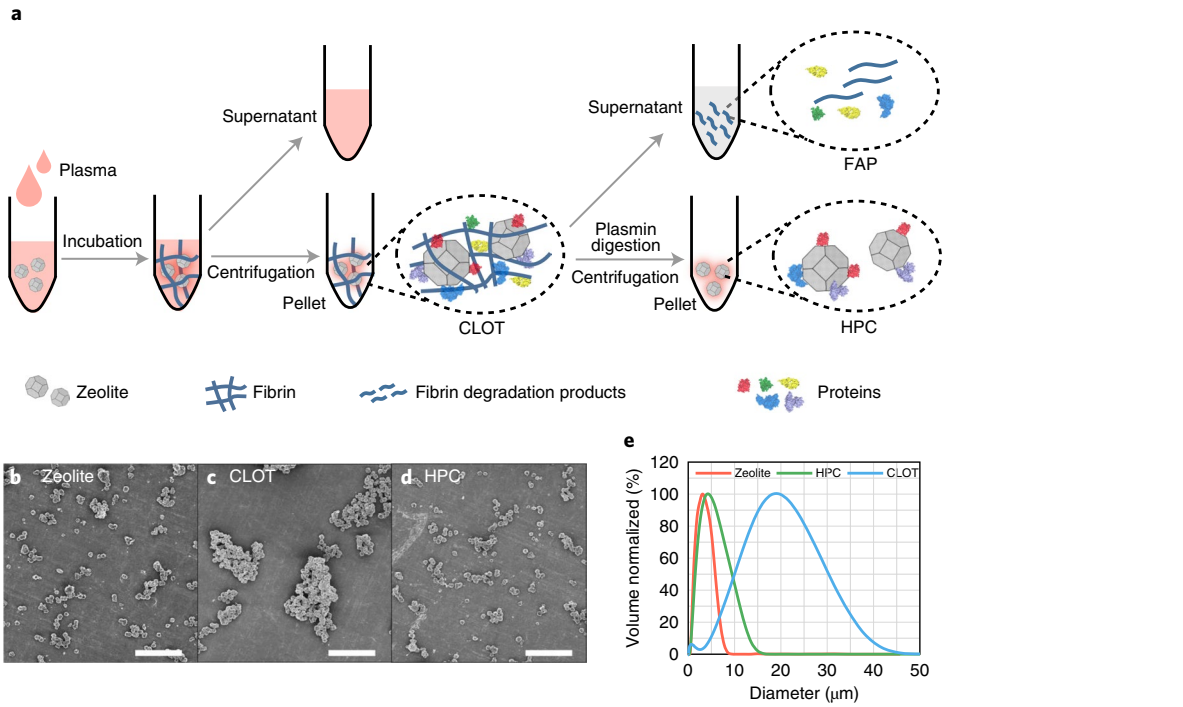

Fig. 1 | Preparation and isolation of the HPC. a, Schematic of the steps from pre-treatment to plasma clot induced by zeolite particles and follow-up proteomic analysis. Zeolite particles with HPC were isolated from plasma clots by plasmin-catalysed fibrinolysis. **b**–**e**, Scanning electron microscopy (repeated at least three times with similar results) (**b**–**d**) and laser diffraction particle sizing analysis (**e**) of zeolite, CLOT and HPC, respectively. Scale bars, 20 μm. The size characterization confirmed that dispersed zeolites with HPC only were recovered.

zeolite-specific coagulation pathway in which the evolving bio–zeolite interface activates and regulates the zymogen (prothrombin) in a way that enhances proteolytic activity. The zeolite complex thus acts as a type of reinforced activated inorganic platelet.

Results

Isolation and characterization of the HPC. Following the incubation of haemostatic Ca-zeolite particles with plasma under physiological conditions, the activated coagulation cascade eventually leads to the generation of thrombin, which cleaves fibrinogen to fibrin monomers, and these then crosslink to form an insoluble clot[28,29]. This process results in the wrapping of zeolite particles by polymerized fibrin fibres, making conventional isolation processes (such as centrifugation or affinity column separation) unsuitable. We thus developed a specific protocol to isolate zeolite particles with HPC for further proteomic analysis, as illustrated in Fig. 1.

First, the ratio of zeolite to plasma was optimized to reduce the relative amount of fibrin, while still keeping the coagulation system functional (Supplementary Table 2). Zeolite/fibrin complexes (denoted as CLOT) with dimensions of 10–30 μm were obtained after breaking the whole clot by vortex mixing for 5 min. We then used plasmin-catalysed fibrinolysis to eliminate the fibrin from these CLOT fragments[30], as shown in Fig. 1 and Supplementary Fig. 2. After 2 h of digestion with plasmin, the CLOT fragments were broken into highly dispersed particles with a diameter of ~3 μm, close to the size of bare zeolite (2.7 μm). The right shift measured by laser diffraction particle analysis (Fig. 1e) is consistent with the formation of a thin protein layer around the zeolites, indicating that dispersed zeolites with HPC (only) were successfully isolated.

The resultant fibrin degradation products and other fibrin-attached proteins residing in the supernatant after fibrinolysis (denoted as FAP) were also collected together. All the samples (CLOT, HPC and FAP) were then subjected to liquid chromatography with tandem mass spectrometry (LC-MS/MS), and raw mass spectra files were searched against the human protein database. The proteins identified were classified according to their biological function (Fig. 2a and Supplementary Table 3). A full list of the proteins identified is provided in Source Data Fig. 2.

The protein composition of the HPC is notably different from that of FAP and crude plasma. One noticeable difference observed between HPC and FAP is that serum albumin is the most abundant protein species in FAP, accounting for 29.1% in total protein. HPC has a much lower amount of serum albumin (6.5%), but a high concentration of fibrinogen (33.7%), which is consistent with previous reports that the zeolite surface promotes preferential adsorption of fibrinogen over serum albumin in full plasma[31,32]. The HPC has a unique protein composition. Specifically, complement and coagulation proteins are remarkably enriched in the HPC compared to crude plasma (Fig. 2a). The total amount of coagulation proteins in the HPC is as high as 3.1%, compared to 0.8% in crude plasma ($P < 0.05$), indicating strong interactions between the zeolite surface and coagulation proteins. In addition, a full set of intrinsic pathway coagulation factors (including factors V, IX, X, XI and XII) are identified in the HPC of zeolites. Most coagulation factors (II, V, X, XI and XII) are found to be concentrated by a factor of 3–400 in the HPC compared to crude plasma (Fig. 2c and Supplementary Table 4). This is a strong indication that the coagulation cascade might be catalysed by the concentrated coagulation factors presented onto the zeolite surface. In living organisms, most catalytic reactions of the coagulation cascade occur on the surface of cells (platelets)[4]. We therefore hypothesize that the concentrated coagulation factors on the zeolite surface (in the HPC) may have similar biological functions, like those in the conventional coagulation process that takes place in crude plasma. In particular, factors X and V are enriched by over two orders of magnitude, directly contributing to the key step of thrombin activation (Fig. 2d). This hypothesis will be tested in the next section.

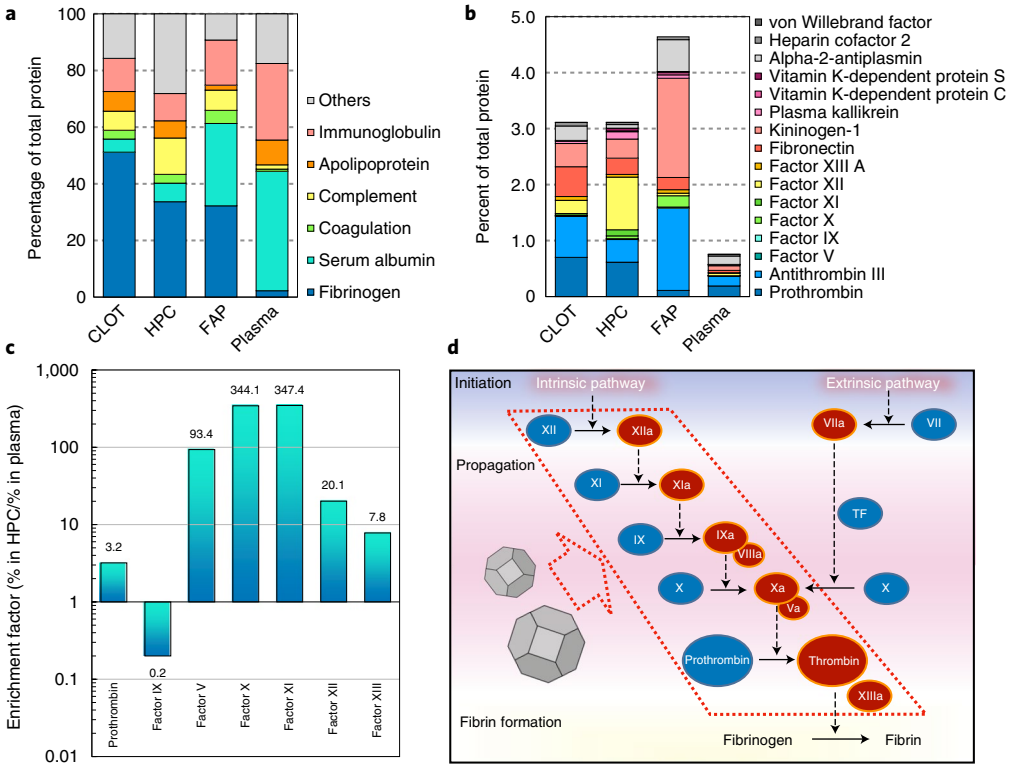

Fig. 2 | Protein analysis. a, Histogram of functional groups. **b**, Coagulation proteins as identified by MS. The HPC was shown to have a unique protein composition, with a particularly high abundance of fibrinogen and coagulation factors. **c**, Enrichment factor (% in HPC/% in plasma) of coagulation factors in HPC over plasma. **d**, Schematic of the effect of zeolite on the intrinsic coagulation pathway.

Dynamic process of zymogen activation in the HPC. Conventionally, thrombin is generated through cleavage of prothrombin by a membrane-bound prothrombinase complex, which assembles factors Xa and Va on the lipid bilayer membrane surface of a platelet[33,34]. Considering the enrichment level of factor V and factor X found on the zeolite surface, we hypothesized that the inorganic surface of the zeolite might coordinate and assemble a prothrombinase complex (Fig. 3). To verify this hypothesis, we first conducted a time-resolved quantitative analysis of factors V and X on the zeolite (in HPC) using an enzyme-linked immunosorbent assay (ELISA) and monitored the activation of thrombin by quantitative western blot (Fig. 3). As shown in Fig. 3, factors V and X accumulated on the zeolite surface in the first 5 min, followed by a thrombin burst between 7 and 10 min. Eventually, the fibrin clot formed at around 12 min, indicating the end of coagulation. These entire dynamic processes can be separated into three stages: (1) coagulation factors complex assembly, (2) thrombin burst and (3) fibrin clot formation.

The coincidence of enrichment of factors V and X in the HPC of the zeolite and the subsequent burst of thrombin support the hypothesis that factors V and X form an active prothrombinase complex on the zeolite surface. To further confirm this assumption, the zeolite protein corona composites formed at different time points (denoted as HPC/Zeo-*x* min) in the first step (coagulation factors complex assembly) were collected and then incubated with prothrombin, and thrombin generation was monitored by quantitative western blot at 20-min intervals to evaluate prothrombinase activity (Fig. 4a).

As depicted in Fig. 4a, HPC/Zeo-*x* min is able to independently convert prothrombin to thrombin. Figure 4b shows that the generated thrombin is directly related to the consumption of prothrombin. HPC/Zeo-5 min exhibits a much higher thrombin generation rate than HPC/Zeo-1 min (0.42 versus 0.03 ng min^{-1}), indicating accumulated prothrombinase activity on the zeolite surface during this period (Fig. 4c). The prothrombinase complex was thus successfully shown to be assembled on the zeolite surface and to functionally contribute to thrombin activation during haemostasis. However, it is not currently clear how factors V and X are activated to form prothrombinase. Compared to the biological membranes (such as a platelet) that are responsible for binding prothrombinase in vivo, the zeolite surface exhibits similar functions. Both surfaces are negatively charged and the zeolite itself contains calcium cations, which are necessary for prothrombinase assembly. The replacement of Ca^{2+} with Na^{+} results in the failure of thrombin generation, as confirmed in our previous study[16].

Unusual thrombin activation patterns in the HPC. The zeolite surface is primed to coordinate the assembly of the prothrombinase (factors Xa/Va) complexes and subsequently localizes and controls the burst of thrombin generation. This bio–inorganic hybrid complex shows completely different thrombin activation patterns, thus profoundly affecting fibrin clot formation. Unlike the classic cell-based model, where thrombin molecules activated on platelet surfaces are released into the solution phase of plasma[35], most zeolite-activated thrombin molecules are captured by the zeolites and localized on the zeolite surface. We employed a quantitative western blot to investigate the distribution of thrombin between the HPC and FAP. As shown in Fig. 5a,b, over 90.6% of the thrombin was located in the HPC, as opposed to the FAP. The amount of thrombin was estimated to be 0.5% in the total protein of the HPC, with an activity of ~1,300 NIH U mg^{-1} by chromogenic substrate assay.

Zeolite-initiated thrombin generation was followed by the use of chromogenic substrates, revealing a striking characteristic pattern. In contrast to the conventional coagulation process, where

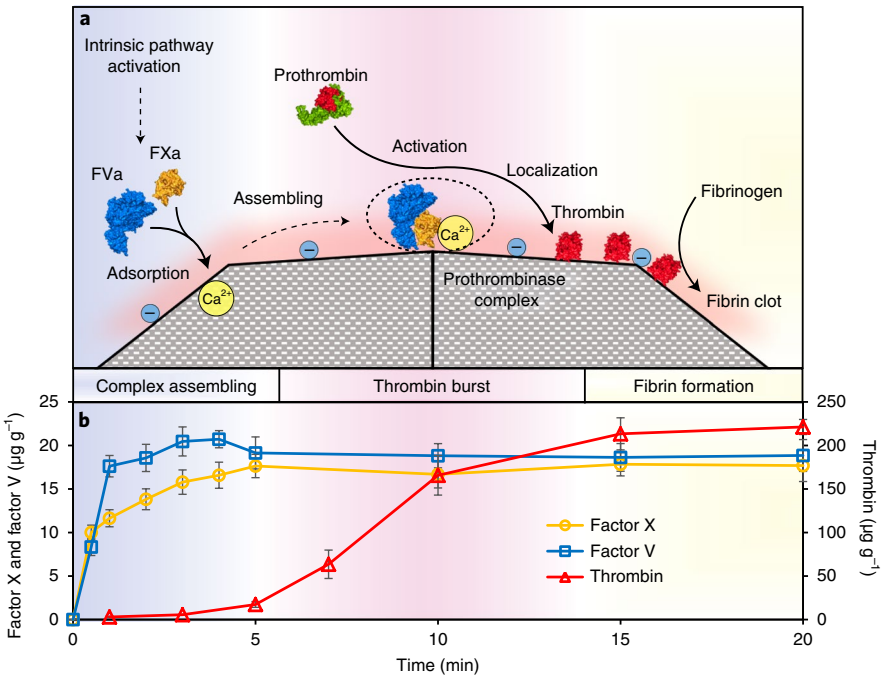

Fig. 3 | Dynamic process of prothrombinase complex (factors X and V) assembly on the zeolite surface. a,**b**, Schematic of prothrombinase complex assembly and thrombin activation (**a**) and quantitative monitoring of factor V, factor X and thrombin (**b**) over the course of the coagulation process on the zeolite. Data values correspond to mean ± s.d., $n = 3$ biologically independent samples.

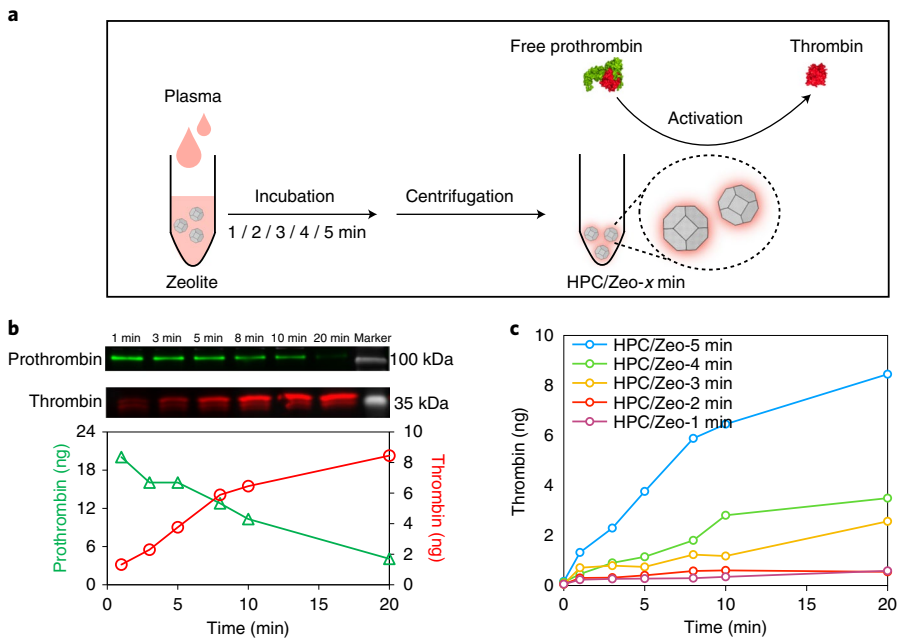

Fig. 4 | Activation of prothrombin to thrombin by HPC/Zeo. a, Zeolite was incubated with plasma for 1–5 min and then isolated (denoted as HPC/Zeo-*x* min). **b**, The catalytic performance of HPC/Zeo-5 min was investigated with a prothrombin-to-thrombin conversion assay monitored by quantitative western blot (repeated twice with similar results). **c**, Prothrombin-to-thrombin transformation curves of HPC/Zeo-*x* min samples, suggesting a positive correlation between the incubation time (*x* min) and the thrombin activation rates.

the thrombin generation profile exhibits a peak when the rates of thrombin production and thrombin inhibition reach equilibrium[3], the thrombin generation profile of zeolite-initiated coagulation exhibits a plateau following the large burst of thrombin generation (Fig. 5c). There is no obvious decline of thrombin activity at 60 min, whereas a return to baseline within 30 min is found in a normal physiological (non-zeolite) system (Fig. 5c). There are two remarkable features in the activation pattern of zeolite-initiated thrombin generation: (1) the plateau activity is notably higher (threefold) than the peak activity without zeolite initiation and (2)

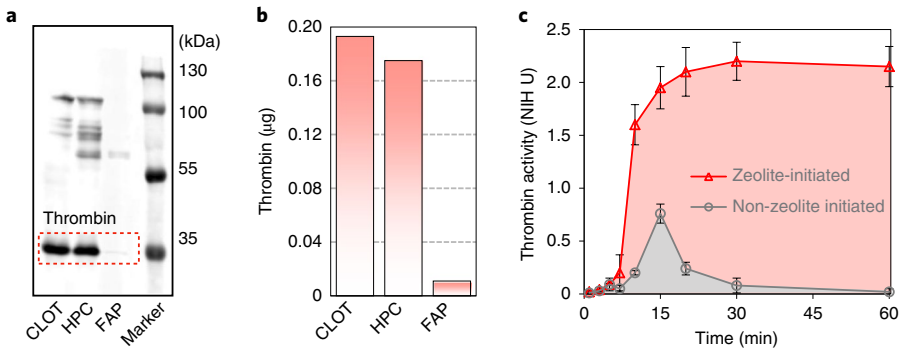

Fig. 5 | Evaluation of thrombin initiated by zeolite. a, Quantitative immunoblot assay of thrombin (repeated at least three times with similar results). **b**, Over 90% of thrombin was located in the HPC on the zeolite surface. **c**, Zeolite-initiated coagulation resulted in a much higher ETP (108.9–8.675 NIH U min) in the HPC on the zeolite surface compared to a non-zeolite-initiated process. Data values correspond to mean ± s.d., $n = 3$ biological independent samples.

the total amount of free thrombin measured during the reaction course, which is referred to as the area under the curve (AUC) or endogenous thrombin potential (ETP)[36], is 12-fold higher than that of the common physiological (non-zeolite) process, functionalized as reinforced inorganic platelets. The notably enhanced plateau activity and ETP of zeolite-initiated thrombin generation is also confirmed in the presence of tissue factor (Supplementary Fig. 6). Compared to a normal plasma clot, in which thrombin has a self-limited lifetime regulated by the body coagulation system balance[37,38], the thrombin in the HPC on zeolite showed exceptional stability even against antithrombin inhibition[16], resulting in an accumulated superior proteolytic activity. There are two features that may prevent thrombin inhibition. First, conformation changes, as characterized in the following section, may alter its interaction with antithrombin and subsequently cleave its reactive bait loop. Second, the solid zeolite surface may restrict the approaching inhibitor so that it can only bind to the thrombin through limited orientations. This thrombin activation pattern distinguishes zeolite-initiated coagulation from platelet-based thrombin generation systems and has a profound impact on fibrin clot formation and haemostasis.

Conformation-regulated enhanced thrombin activity. The greatly reinforced biofunction is associated with the evolving bio–zeolite interface activating zymogen and regulating the enzymes in a way that enhances proteolytic activity. A quantitative analysis of thrombin activity was carried out in a modelled thrombin/zeolite system. To simplify the complex physiological system, we chose albumin, which is the most abundant protein in plasma and accelerates the onset of fibrin clot formation to simulate a plasma environment[5,39,40]. Zeolite with bovine serum albumin (BSA) adsorbed on its surface (BSA@Zeo) showed a remarkable reduction of zeta potential and a similar polydispersity index (PDI) to zeolite (Supplementary Fig. 8). The catalytic activity of thrombin was characterized using a chromogenic substrate (S2238). As shown in Fig. 6a, the slope of the fitting curve represents the catalytic activity of thrombin (the kinetic study of thrombin catalytic activity is discussed in the Supplementary Methods). This reveals that the direct adsorption of thrombin on the zeolite surface (Thr@Zeo) leads to a complete deactivation (Fig. 6a)[16]. However, the pre-adsorption of BSA successfully prevents the deactivation of thrombin, and the activity of thrombin/BSA co-adsorbed on the zeolite surface (Thr-BSA@Zeo) is nearly three times as high as that of free thrombin (slope of 0.811 versus 0.306, Fig. 6a). It is interesting to note that the plateau thrombin activity of zeolite-initiated coagulation is also three times as high as the peak activity in conventional (non-zeolite) plasma coagulation. These results imply that the protein corona on the zeolite surface may play an important role in regulating thrombin activity.

The notable enhancement of thrombin activity probably relates to its conformation on the zeolite surface. It is widely accepted that there are fluctuations between conformations in many enzymes. The equilibrium of these conformations may be responsible for the binding and release of the substrate[41]. An active dimethyl labelling strategy combined with MS was applied to systematically probe the lysine-proximal microenvironments of the thrombin/zeolite complexes, based on the fact that free lysine residues on the enzyme exterior surfaces are more easily and quickly accessed and labelled than those engaged in strong enzyme-to-zeolite interactions[42]. A significant reduction in Thr@Zeo was observed, not only in the labelling levels of K459 and K618, both of which were near or included in the exosite II region of the thrombin, but also in K330, K443 and K440 around exosite I (Fig. 6b and Supplementary Table 5), indicating that their surroundings were blocked by the zeolite surface. Because the exosites play an important role in the stabilization of the initial thrombin–substrate complexes[43], the blocking of exosite I and exosite II would be a possible explanation for the loss in activity of Thr@Zeo. On the other hand, the total labelling level increased significantly in Thr-BSA@Zeo, even compared to free thrombin (71% versus 66%), indicating a looser surface structure. In particular, K501 exhibited doubled labelling levels (Fig. 6c and Supplementary Table 5), indicating enhanced accessibility to the surrounding surface residues. Because the chromogenic substrate used in this experiment (S2238) was directly bound to the thrombin active site[44], the looser structure of surface residues may lead to increased opportunities for the small substrate to contact the active site (Fig. 6b), which could be a possible reason for the higher catalytic activity shown by Thr-BSA@Zeo.

Thrombin adsorbed on another zeolite (CaA) with a much lower Si/Al ratio (1.0 versus 2.6) showed almost identical catalytic performance (Supplementary Fig. 9), indicating that a similar conformation change may be observed for Thr@CaA and Thr@Zeo. Thr@CaA also showed a significant reduction of the total labelling level as well as the labelling levels of K459 and K618 (Supplementary Table 6), indicating the blocking of exosite II. Moreover, Thr-BSA@CaA exhibits a similar looser structure. However, there still remain some differences among the labelling levels of specific sites (Supplementary Table 6). It should be noted that only two types of zeolite were investigated as part of the work reported in this Article, so there is a need for further systematic study of the effect of zeolite composition and structure on thrombin adsorption. It has been shown that the calcium content in the zeolite plays an important role in regulating their catalytic performance in the HPC (Supplementary Fig. 11).

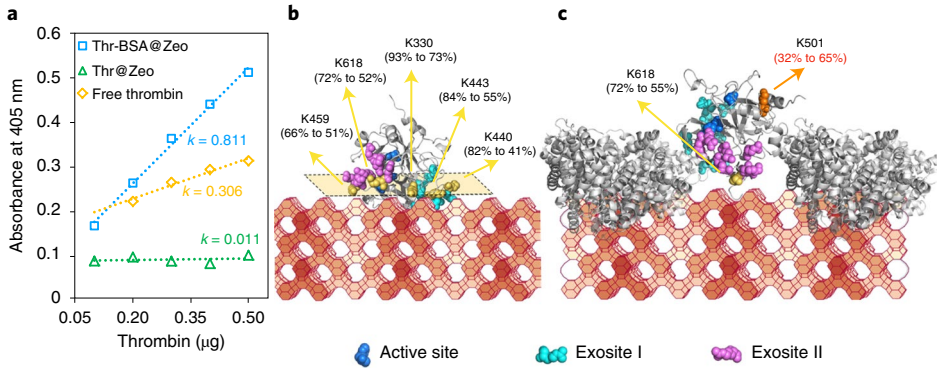

Fig. 6 | The unique conformation and enhanced activity of thrombin on zeolite. a, A catalytic kinetic study revealed the different performance of the zeolite-immobilized thrombin. **b**, Schematic of Thr@Zeo and lysine sites, indicating significant changes in the labelling level and the possible conformation of thrombin on the zeolite surface. **c**, Schematic of Thr-BSA@Zeo and lysine sites, showing significant changes in the labelling level and the possible conformation of thrombin on the zeolite surface. Pre-adsorption of albumin (in grey) on the zeolite surface would lead to an open state of the active site, increasing the probability of interaction with substrate.

Discussion

The haemostatic application of zeolites has been of interest for more than three decades, but the understanding of its mechanism has remained limited to basic physiochemical properties[13,45], and the interaction between the inorganic surface and functional proteins has been poorly investigated so far. Through continuous monitoring of the evolving zeolite corona in the course of the coagulation reaction, we reveal that the zeolite effectively initiates and propagates the coagulation cascade via the intrinsic coagulation pathway. In addition to localization of coagulation factors, the zeolite surface is primed to coordinate an assembly of the prothrombinase (factors Xa/Va) complexes and subsequently localizes and controls the burst of thrombin generation leading to fibrin clot formation, in a similar fashion to platelet-initiated coagulation. Based on these findings, we propose a surface-based model for zeolite-initiated haemostasis consisting of three main steps: (1) initiation and procoagulant complex assembly, which occurs on the negatively charged zeolite surface via an intrinsic pathway to set the stage for large-scale thrombin generation, (2) thrombin burst, in which large amounts of thrombin are generated on site on the zeolite surface, catalysed by the procoagulant complex and (3) fibrin clot formation. It should be noted that the separation is useful in this regard due to the involvement of many proteins and protein-to-zeolite interactions in these dynamics, but it is artificial. In fact, each stage is initiated in rapid succession, and each continues until the trigger for that stage is no longer present, so there is overlap.

The surface-based model of zeolite-initiated coagulation proposed in this work explains important aspects that were overlooked in protein-concentration models. We have demonstrated that the zeolite provides a surface for activation of the intrinsic pathway and coagulation complex assembly. This regulation extends beyond surface activation via the glass effect, which has been observed for kaolin[46], and enables assembly of a coagulation complex that contributes to the promotion and control of thrombin generation and localization. This model provides a rational explanation for the critical role of Ca^{2+} in the zeolite haemostatic agent. Although other cation-exchanged zeolites show similar water adsorption properties, an absence of Ca^{2+} ions precludes the formation of the prothrombinase complex on the zeolite surface and results in a failure of zeolite-surface thrombin generation and in the formation of ineffective clots[33]. This mechanism may not be entirely restricted to the zeolite surface, although only one type of zeolite was investigated here, and the process of prothrombin activation may occur on other surfaces that are negatively charged in the presence of calcium ions.

Furthermore, in stark contrast to the cell-based physiological process, the prothrombin-to-thrombin conversion in the HPC of the Ca-zeolite displays a striking thrombin activation pattern with an exceptionally high plateau thrombin activity and at least 12-fold enhanced ETP. The more efficient zymogen activation on the zeolite surface means it is functionalized as a reinforced inorganic platelet to treat large injuries where platelets fail to initiate a stable clot[6]. It should be noted that, for practical applications, powdered zeolite material may enter the systemic system and cause thromboembolic events. To address this challenge, as reported in a previous study, we have developed a tightly bonded and flexible mesoporous zeolite–cotton hybrid haemostat to eliminate the risk of zeolitic powder entering the patient's body[14].

Methods

Isolation and characterization of the HPC. *Human plasma.* Human blood from healthy volunteers was collected in plastic tubes containing sodium citrate to prevent blood clotting. The tubes were centrifuged to obtain platelet-poor plasma (PPP). The PPP was transferred to labelled tubes and stored at −20 °C until use. The procedures for obtaining human blood samples were carried out in accordance with the ethical regulations of Zhejiang University (ZJU). The Department of Chemistry (ZJU) approved the study protocol. Informed consent was obtained from all participants.

Plasma incubation. As an optimized ratio (Supplementary Table 2), 10 mg of calcium-exchanged zeolite[16] was incubated with 30 μl of plasma, 3 μl of $CaCl_2$ solution (0.2 M) and 70 μl of HEPES buffer (20 mM HEPES, 150 mM NaCl, pH 7.4) on a thermoshaker at 37 °C for 30 min. Excessive plasma was then removed and the clot was washed with 200 μl of HEPES buffer three times.

Fibrinolysis by plasmin. For the HPC sample, washed pellets were resuspended in 100 μl of human plasmin (25 μg ml^{-1}) to conduct fibrinolysis at 37 °C for 0–120 min before protein extraction. Afterwards, the supernatant (denoted as SUP) was collected, and the remaining pellet was further subjected to protein extraction.

Protein extraction. The pellets of CLOT or HPC were resuspended in 100 μl of guanidine hydrochloride (6 M) and heated at 90 °C for 5 min to extract proteins. The supernatant was collected and the extraction repeated three times. The protein solution was then concentrated using a protein concentrator with a molecular weight cutoff (MWCO) of 3 kDa until guanidine hydrochloride was diluted until lower than 20 mM. The buffer was replaced by an ammonia bicarbonate buffer (20 mM NH_4HCO_3, pH 8.0).

Dynamic process of zymogen activation in the HPC. *Monitoring of factor X/factor V assembly and the thrombin activation process.* Calcium-exchanged zeolite[16] (10 mg CaY, with Si/Al of 2.6) was incubated with 30 μl of plasma, 3 μl of $CaCl_2$ solution (0.2 M) and 70 μl of HEPES buffer (20 mM HEPES, 150 mM NaCl, pH 7.4) on a thermoshaker at 37 °C for 0.5–20 min. At each time point of 0.5, 1, 2, 3, 4, 5, 10, 15 and 20 min, excessive plasma supernatant was removed after centrifugation and sent for factor X or factor V ELISA assay.

The particles were washed with 200 µl of HEPES buffer three times, then resuspended in 135 µl of HEPES buffer; 135 µl 2% SDS and 67.5 µl 5× loading buffer were then added into the tube, which was incubated on a thermoshaker at 99 °C for 10 min. Samples (10 µl) were loaded into each well to conduct gel electrophoresis as mentioned above, then sent for quantitative western blot.

ELISA assay. An FX Human ELISA kit (ab108832, Abcam) and FV Human ELISA kit (ab137976, Abcam) were used. Plasma incubation was conducted as mentioned above on a thermoshaker at 37 °C for 1–20 min. The supernatant was used to conduct ELISA assays after centrifugation and dilution by 1× diluent N to a final dilution of 1:800. The amounts of factor X and factor V adsorbed on the zeolite were calculated by subtracting the remaining factor X or factor V in the supernatant from that in the original plasma.

Quantitative western blot. The gel obtained after electrophoresis was transferred to a polyvinylidene difluoride (PVDF) membrane using a Bio-Rad Mini Trans-Blot system at 250 mA for 2 h. The membrane was blocked with blocking buffer (Beyotime QuickBlock Western) for 30 min, and incubated with primary antibody (antithrombin, ab17199, Abcam) overnight at 4 °C. The membrane was washed with Tris-Buffered Saline Tween-20 (TBS-T) buffer and incubated with secondary antibody (anti-mouse immunoglobulin G DyLight 800, Cell Signaling Technology) at 25 °C for 1 h. The membrane was washed thoroughly with TBS-T and imaged by an Odyssey CLx Imager (LI-COR). The image was quantitatively analysed using Image Studio Lite (LI-COR) software. Pure human thrombin (Sigma T6884) was used as reference (Supplementary Fig. 3).

Unusual thrombin activation patterns in the HPC. *Thrombin generation assay without tissue factor.* Only $CaCl_2$ was used as a trigger in this experiment.

In a typical zeolite-initiated thrombin generation assay, 10 mg of calcium-exchanged zeolite (CaY, Si/Al of 2.6) was incubated with 30 µl of plasma, 3 µl of $CaCl_2$ solution (0.2 M) and 70 µl of HEPES buffer (20 mM HEPES, 150 mM NaCl, pH 7.4) in a tube on a thermoshaker at 37 °C for 1–60 min. After incubation, 15 µl of the zeolite particles suspension was mixed with 255 µl of HEPES buffer and 30 µl of thrombin chromogenic substrate solution (4 mg ml^{-1}, S2238, HYPHEN BioMed)[47]. The reaction was conducted at 37 °C on a thermoshaker for 2 min, then 50 µl of acetic acid was quickly added to stop the reaction. The absorbance of the supernatant was determined at 405 nm. Pure human thrombin was used as reference.

In a typical non-zeolite-initiated thrombin generation assay, 30 µl of plasma, 3 µl of $CaCl_2$ solution (0.2 M) and 70 µl of HEPES buffer (20 mM HEPES, 150 mM NaCl, pH 7.4) were mixed in a tube on a thermoshaker at 37 °C for 1–60 min. After incubation, 15 µl of solution was mixed with 255 µl of HEPES buffer and 30 µl of thrombin chromogenic substrate solution (4 mg ml^{-1}, S2238, HYPHEN BioMed)[47]. The reaction was conducted at 37 °C on a thermoshaker for 2 min, then 50 µl of acetic acid was quickly added to stop the reaction. The absorbance of the supernatant was determined at 405 nm. Pure human thrombin was used as reference.

Conformation-regulated enhanced thrombin activity. *Active dimethyl labelling and conformation analysis.* Sample preparation. Active dimethyl labelling was conducted according to a previous study[42]. In a typical dimethyl labelling assay, samples (free thrombin, Thr@Zeo and Thr-BSA@Zeo) were mixed with 400 µl of HEPES buffer at 37 °C for 30 min (protein concentration was 0.1 mg ml^{-1}), then 3.2 µl of $NaBH_3CN$ (0.6 M) and 3.2 µl of CH_2O (4%) were added and the reaction was carried out at 37 °C for 25 min. To stop the reaction, 4 µl of NH_4HCO_3 (5 M) was added and incubated for 20 min.

For CaA zeolite, 50 µl of HCl (6 M) was added to dissolve the zeolite, and the buffer was then changed to 20 mM NH_4HCO_3 by centrifugal filters (MWCO 3k), followed by freeze-drying. For CaY zeolite, 1 ml of 6 M guanidine chloride was added to extract the protein on the zeolite surface with a 10-min ultrasound step, and the supernatant was collected. This extraction was repeated three times. All of the supernatant was combined, followed by freeze-drying.

The sample was next incubated with 6 M guanidine chloride and 20 mM dithiothreitol at 37 °C for 2 h. The reaction was conducted at 25 °C for 40 min in the dark with 40 mM iodoacetamide (IAA). The reaction was terminated by exposure to light for 20 min.

The salt and guanidine were removed by centrifugal filters (MWCO 3k, change of buffer to 20 mM NH_4HCO_3, pH 8.0) to a final volume of 200 µl. The final concentration of guanidine should be less than 10 mM and ideally less than 5 mM. Digestion was performed by chymotrypsin at 37 °C at an enzyme-to-substrate ratio of 1/25 (wt/wt).

The selection of enzyme was based on the compatibility and recovery rate of the peptides. In this part, chymotrypsin was chosen to achieve a higher recovery rate of peptides.

LC-MS/MS analysis. An EASY-nLC 1000 system (Thermo Fisher) was used for LC-MS/MS analysis. All of the protein samples (injection mass, ~2 µg protein) were separated by a nanoViper capillary column (50 µm, 15-cm length) packed with C18 particles (2 µm, 100 Å). The flow rate was 10 nl min^{-1}. The solution of 0.1% formic acid (FA)/H_2O was used as mobile phase A and 0.1% FA/acetonitrile (ACN) as mobile phase B. Data were acquired with a Thermo Xcalibur 3.0. The LC gradient is shown in Supplementary Table 1.

An LTQ Orbitrap Elite system (Thermo Fisher) was used for MS analysis. The MS parameters were set as follows: ion transfer capillary 275 °C, spray voltage 1.8 kV and full MS scan from m/z 300 to 2,000 with a resolution of 60,000. Data-dependent MS/MS scans were performed by selecting the 20 most intense ions in the full MS scan for collision-induced dissociation with 35.0% normalized collision energy.

All data were searched against the UniProt protein database and analysed with Peak Studio 8.0. Peptides were processed using chymotrypsin cleavage, and up to two missed cleavage sites were allowed. Peptide mass tolerance was 20 ppm and fragment mass tolerance was 0.8 Da.

Reporting Summary. Further information on research design is available in the Nature Research Reporting Summary linked to this Article.

Data availability

All data supporting the findings of this study are available within the Article and its Supplementary Information or from the corresponding authors upon reasonable request. The MS proteomics data have been deposited in the ProteomeXchange Consortium (http://proteomecentral.proteomexchange.org) via the iProX partner repository with the dataset identifier PXD024170. Source data are provided with this paper.

Received: 8 February 2020; Accepted: 16 June 2021;
Published online: 22 July 2021

References

1. Neurath, H. Evolution of proteolytic enzymes. *Science* **224**, 350–357 (1984).
2. Neurath, H. & Walsh, K. A. Role of proteolytic enzymes in biological regulation (a review). *Proc. Natl Acad. Sci. USA* **73**, 3825–3832 (1976).
3. Wolberg, A. S. & Campbell, R. A. Thrombin generation, fibrin clot formation and hemostasis. *Transfus. Apher. Sci.* **38**, 15–23 (2008).
4. Monroe, D. M., Hoffman, M. & Roberts, H. R. Platelets and thrombin generation. *Arterioscler. Thromb. Vasc. Biol.* **22**, 1381–1389 (2002).
5. Wolberg, A. S. Thrombin generation and fibrin clot structure. *Blood Rev.* **21**, 131–142 (2007).
6. Monroe, D. M. & Hoffman, M. What does it take to make the perfect clot? *Arterioscler. Thromb. Vasc. Biol.* **26**, 41–48 (2006).
7. Hickman, D. A., Pawlowski, C. L., Sekhon, U. D., Marks, J. & Gupta, A. S. Biomaterials and advanced technologies for hemostatic management of bleeding. *Adv. Mater.* **30**, 1700859 (2018).
8. Alam, H. B. et al. Application of a zeolite hemostatic agent achieves 100% survival in a lethal model of complex groin injury in swine. *J. Trauma Acute Care Surg.* **56**, 974–983 (2004).
9. Kheirabadi, B. S., Scherer, M. R., Estep, J. S., Dubick, M. A. & Holcomb, J. B. Determination of efficacy of new hemostatic dressings in a model of extremity arterial hemorrhage in swine. *J. Trauma Acute Care Surg.* **67**, 450–460 (2009).
10. Gruen, R. L. et al. Haemorrhage control in severely injured patients. *Lancet* **380**, 1099–1108 (2012).
11. Achneck, H. E. et al. A comprehensive review of topical hemostatic agents: efficacy and recommendations for use. *Ann. Surg.* **251**, 217–228 (2010).
12. Gordy, S. D., Rhee, P. & Schreiber, M. A. Military applications of novel hemostatic devices. *Expert Rev. Med. Devices* **8**, 41–47 (2011).
13. Pourshahrestani, S., Zeimaran, E., Djordjevic, I., Kadri, N. A. & Towler, M. R. Inorganic hemostats: the state-of-the-art and recent advances. *Mater. Sci. Eng. C* **58**, 1255–1268 (2016).
14. Yu, L. et al. A tightly-bonded and flexible mesoporous zeolite–cotton hybrid hemostat. *Nat. Commun.* **10**, 1932 (2019).
15. Granville-Chapman, J., Jacobs, N. & Midwinter, M. Pre-hospital haemostatic dressings: a systematic review. *Injury* **42**, 447–459 (2011).
16. Li, Y. et al. In situ generated thrombin in the protein corona of zeolites: relevance of the functional proteins to its biological impact. *Nano Res.* **7**, 1457–1465 (2014).
17. Tenzer, S. et al. Nanoparticle size is a critical physicochemical determinant of the human blood plasma corona: a comprehensive quantitative proteomic analysis. *ACS Nano* **5**, 7155–7167 (2011).
18. Walkey, C. D. & Chan, W. C. Understanding and controlling the interaction of nanomaterials with proteins in a physiological environment. *Chem. Soc. Rev.* **41**, 2780–2799 (2012).
19. Cedervall, T. et al. Understanding the nanoparticle-protein corona using methods to quantify exchange rates and affinities of proteins for nanoparticles. *Proc. Natl Acad. Sci. USA* **104**, 2050–2055 (2007).
20. Monopoli, M. P., Åberg, C., Salvati, A. & Dawson, K. A. Biomolecular coronas provide the biological identity of nanosized materials. *Nat. Nanotechnol.* **7**, 779–786 (2012).

21. Caracciolo, G. et al. Stealth effect of biomolecular corona on nanoparticle uptake by immune cells. *Langmuir* **31**, 10764–10773 (2015).
22. Dobrovolskaia, M. A. & McNeil, S. E. Immunological properties of engineered nanomaterials. *Nat. Nanotechnol.* **2**, 469–478 (2007).
23. Kelly, P. M. et al. Mapping protein binding sites on the biomolecular corona of nanoparticles. *Nat. Nanotechnol.* **10**, 472–479 (2015).
24. Dawson, K. A. & Yan, Y. Current understanding of biological identity at the nanoscale and future prospects. *Nat. Nanotechnol.* **16**, 229–242 (2021).
25. Jain, P. et al. In-vitro in-vivo correlation (IVIVC) in nanomedicine: is protein corona the missing link? *Biotechnol. Adv.* **35**, 889–904 (2017).
26. Monopoli, M. P. et al. Physical–chemical aspects of protein corona: relevance to in vitro and in vivo biological impacts of nanoparticles. *J. Am. Chem. Soc.* **133**, 2525–2534 (2011).
27. Winzen, S. et al. Complementary analysis of the hard and soft protein corona: sample preparation critically effects corona composition. *Nanoscale* **7**, 2992–3001 (2015).
28. Spahn, D. R. et al. Management of bleeding and coagulopathy following major trauma: an updated European guideline. *Crit. Care* **17**, R76 (2013).
29. Chapin, J. C. & Hajjar, K. A. Fibrinolysis and the control of blood coagulation. *Blood Rev.* **29**, 17–24 (2015).
30. Foley, J. H. Plasmin(ogen) at the nexus of fibrinolysis, inflammation and complement. *Semin. Thromb. Hemost.* **43**, 135–142 (2017).
31. Laurent, S. et al. Corona protein composition and cytotoxicity evaluation of ultra-small zeolites synthesized from template free precursor suspensions. *Toxicol. Res.* **2**, 270–279 (2013).
32. Rahimi, M. et al. Zeolite nanoparticles for selective sorption of plasma proteins. *Sci. Rep.* **5**, 17259 (2015).
33. Krishnaswamy, S. The transition of prothrombin to thrombin. *J. Thromb. Haemost.* **11**, 265–276 (2013).
34. Ivanciu, L., Krishnaswamy, S. & Camire, R. M. New insights into the spatiotemporal localization of prothrombinase in vivo. *Blood* **124**, 1705–1714 (2014).
35. Crawley, J., Zanardelli, S., Chion, C. & Lane, D. The central role of thrombin in hemostasis. *J. Thromb. Haemost.* **5**, 95–101 (2007).
36. Allen, G. A. et al. Impact of procoagulant concentration on rate, peak and total thrombin generation in a model system. *J. Thromb. Haemost.* **2**, 402–413 (2004).
37. Lane, D. A., Philippou, H. & Huntington, J. A. Directing thrombin. *Blood* **106**, 2605–2612 (2005).
38. Tomaiuolo, M., Brass, L. F. & Stalker, T. J. Regulation of platelet activation and coagulation and its role in vascular injury and arterial thrombosis. *Interv. Cardiol. Clin.* **6**, 1–12 (2017).
39. Wilf, J., Gladner, J. A. & Minton, A. P. Acceleration of fibrin gel formation by unrelated proteins. *Thromb. Res.* **37**, 681–688 (1985).
40. Torbet, J. Fibrin assembly in human plasma and fibrinogen/albumin mixtures. *Biochemistry* **25**, 5309–5314 (1986).
41. Daniel, R. M., Dunn, R. V., Finney, J. L. & Smith, J. C. The role of dynamics in enzyme activity. *Annu. Rev. Biophys. Biomol. Struct.* **32**, 69–92 (2003).
42. Zhou, Y. et al. Probing the lysine proximal microenvironments within membrane protein complexes by active dimethyl labeling and mass spectrometry. *Anal. Chem.* **88**, 12060–12065 (2016).
43. Huntington, J. Molecular recognition mechanisms of thrombin. *J. Thromb. Haemost.* **3**, 1861–1872 (2005).
44. Ricci, C. G., Pinto, A. F. M., Berger, M. & Termignoni, C. A thrombin inhibitor from the gut of *Boophilus microplus* ticks. *Exp. Appl. Acarol.* **42**, 291–300 (2007).
45. Hursey, F. X. & Dechene, F. J. Method of treating wounds. US patent 4,822,349 (1989).
46. Ostomel, T. A., Stoimenov, P. K., Holden, P. A., Alam, H. B. & Stucky, G. D. Host–guest composites for induced hemostasis and therapeutic healing in traumatic injuries. *J. Thromb. Thrombolysis* **22**, 55–67 (2006).
47. Sloan, I. G. & Firkin, B. G. Effects of EACA on thrombin generation as measured by the chromagen S2238. *Thromb. Res.* **44**, 761–769 (1986).

Acknowledgements

J.F. acknowledges support from the National Natural Science Foundation of China (91545113, 91845203 and 92045301), China Postdoctoral Science Foundation (2017M610363 and 2018T110584), Shell Global Solutions International BV (PT71423 and PT74557), Fok Ying Tong Education Foundation (131015) and the Science & Technology Program of Ningbo (2017C50014). K.A.D. acknowledges that this publication has emanated from research supported in part by grants from Science Foundation Ireland (17/NSFC/4898 and 17/ERCD/4962) and also from funding under Guangdong Provincial Education Department Key Laboratory of Nano-Immunoregulation Tumor Microenvironment (2019KSYS008). V.C. acknowledges support from the Irish Research Council (GOIPD/2016/128). L.B. acknowledges financial support from the EU H2020 Nanofacturing project (grant agreement no. 646364). V.P. acknowledges financial support from CALIN. We thank Q. Gao for helping with proteomic analysis and protein structure analysis.

Author contributions

J.F. and K.A.D. conceived the project. J.F., K.A.D., X.S. and H.C. designed the experiments and wrote the manuscript. X.S. and H.C. carried out the experiments and data analysis. K.L., V.C., L.B. and V.P. helped with the protein corona MS analysis. M.H. and F.W. helped with the protein conformation analysis. L.X. and L.Y. helped with revision of the manuscript. All authors discussed the results and contributed to the manuscript.

Competing interests

The authors declare no competing interests.

Additional information

Supplementary information The online version contains supplementary material available at https://doi.org/10.1038/s41929-021-00654-6.

Correspondence and requests for materials should be addressed to K.A.D. or J.F.

Peer review information *Nature Catalysis* thanks Russell Morris, Ivan D Tarandovskiy and the other, anonymous, reviewer(s) for their contribution to the peer review of this work.

Reprints and permissions information is available at www.nature.com/reprints.

Publisher's note Springer Nature remains neutral with regard to jurisdictional claims in published maps and institutional affiliations.

nature research

Corresponding author(s): Jie Fan; Kenneth A. Dawson

Last updated by author(s): May 29, 2021

Reporting Summary

Nature Research wishes to improve the reproducibility of the work that we publish. This form provides structure for consistency and transparency in reporting. For further information on Nature Research policies, see Authors & Referees and the Editorial Policy Checklist.

Statistics

For all statistical analyses, confirm that the following items are present in the figure legend, table legend, main text, or Methods section.

n/a	Confirmed
☐	☒ The exact sample size (*n*) for each experimental group/condition, given as a discrete number and unit of measurement
☐	☒ A statement on whether measurements were taken from distinct samples or whether the same sample was measured repeatedly
☒	☐ The statistical test(s) used AND whether they are one- or two-sided *Only common tests should be described solely by name; describe more complex techniques in the Methods section.*
☐	☒ A description of all covariates tested
☒	☐ A description of any assumptions or corrections, such as tests of normality and adjustment for multiple comparisons
☐	☒ A full description of the statistical parameters including central tendency (e.g. means) or other basic estimates (e.g. regression coefficient) AND variation (e.g. standard deviation) or associated estimates of uncertainty (e.g. confidence intervals)
☐	☒ For null hypothesis testing, the test statistic (e.g. *F*, *t*, *r*) with confidence intervals, effect sizes, degrees of freedom and *P* value noted *Give P values as exact values whenever suitable.*
☒	☐ For Bayesian analysis, information on the choice of priors and Markov chain Monte Carlo settings
☒	☐ For hierarchical and complex designs, identification of the appropriate level for tests and full reporting of outcomes
☒	☐ Estimates of effect sizes (e.g. Cohen's *d*, Pearson's *r*), indicating how they were calculated

Our web collection on statistics for biologists contains articles on many of the points above.

Software and code

Policy information about availability of computer code

Data collection	Image Studio Lite (LI-COR) Ver 5.2; Thermo Xcalibur 3.0;
Data analysis	Image Studio Lite (LI-COR) Ver 5.2; Origin 2021; Peak Studio 8.0; Image J 1.8.0; Microsoft Excel.

For manuscripts utilizing custom algorithms or software that are central to the research but not yet described in published literature, software must be made available to editors/reviewers. We strongly encourage code deposition in a community repository (e.g. GitHub). See the Nature Research guidelines for submitting code & software for further information.

Data

Policy information about availability of data

All manuscripts must include a data availability statement. This statement should provide the following information, where applicable:

- Accession codes, unique identifiers, or web links for publicly available datasets
- A list of figures that have associated raw data
- A description of any restrictions on data availability

All the data supporting the findings of this study are available within the article and its Supplementary Information or from the corresponding authors upon reasonable request. The source data underlying Figs. 1e, 2a, 2b, 2c, 3, 4b, 4c, 5a, 5b, 5c and 6a are provided as a Source Data file; and the source data underlying Supplementary Figs. 2g, 3b, 3d, 6, 8a, 9 and 11 are provided as an Additional Supplementary File. The mass spectrometry proteomics data have been deposited in the ProteomeXchange Consortium (http://proteomecentral.proteomexchange.org) via the iProX partner repository with the dataset identifier PXD024170.

Field-specific reporting

Please select the one below that is the best fit for your research. If you are not sure, read the appropriate sections before making your selection.

☒ Life sciences ☐ Behavioural & social sciences ☐ Ecological, evolutionary & environmental sciences

For a reference copy of the document with all sections, see nature.com/documents/nr-reporting-summary-flat.pdf

Life sciences study design

All studies must disclose on these points even when the disclosure is negative.

Sample size	For the data involved statistical analysis, the sample size were made to be two/three biological independent assay.
Data exclusions	No data were excluded from the analyses.
Replication	All the experiments were performed in two/three or more replication. Data were repeated on different date.
Randomization	The allocation of samples were random.
Blinding	The investigators were blinded to group allocation during data collection and/or analysis.

Reporting for specific materials, systems and methods

We require information from authors about some types of materials, experimental systems and methods used in many studies. Here, indicate whether each material, system or method listed is relevant to your study. If you are not sure if a list item applies to your research, read the appropriate section before selecting a response.

Materials & experimental systems

n/a	Involved in the study
☐	☒ Antibodies
☒	☐ Eukaryotic cell lines
☒	☐ Palaeontology
☒	☐ Animals and other organisms
☐	☒ Human research participants
☒	☐ Clinical data

Methods

n/a	Involved in the study
☒	☐ ChIP-seq
☒	☐ Flow cytometry
☒	☐ MRI-based neuroimaging

Antibodies

Antibodies used

Primary:
Thrombin primary antibody （ab17199, Abcam, Mouse monoclonal [5G9] to Thrombin, reacts with: Cow, Human） at 1/500 dilution;
Human Factor X ELISA Kit (ab108832, Abcam, reacts with: Human, assay type: Sandwich);
Human Factor V ELISA Kit (ab137976, Abcam, reacts with: Human, assay type: Sandwich);
Secondary:
Anti-mouse IgG (H+L) DyLight™ 800 (#5257, Cell Signaling Technology, prepared from goat antibodies) at 1/15000 dilution;

Validation

Thrombin primary antibody:
ab17199, Abcam, species reactivity: cow, human;
application: ELISA; WB; IHC-P;
More detailed information may be found here (online database): https://www.abcam.com/thrombin-antibody-5g9-ab17199.html

Human Factor X ELISA Kit:
ab108832, Abcam, species reactivity: human;
assay type: Sandwich (quantitative);
sample type: Cell culture supernatant, Saliva, Milk, Urine, Serum, Plasma;
More detailed information may be found here (online database): https://www.abcam.com/human-factor-x-elisa-kit-ab108832.html

Human Factor V ELISA Kit:
ab137976, Abcam, species reactivity: human;

assay type: Sandwich (quantitative);
sample type: Cell culture supernatant, Saliva, Milk, Urine, Serum, Plasma;
More detailed information may be found here (online database): https://www.abcam.com/human-factor-v-elisa-kit-ab137976.html

Human research participants

Policy information about studies involving human research participants

Population characteristics	Aged between 20 to 30 years old, no past and current hematological disease.
Recruitment	Volunteers were recruited from the Zhejiang University.
Ethics oversight	Chemistry Department of Zhejiang University

Note that full information on the approval of the study protocol must also be provided in the manuscript.